Supplementary Information

Dislocation mechanisms in the plastic deformation of monodisperse wet foams within an expansion-contraction microfluidic geometry

Daniel Vecchiolla and Sibani Lisa Biswal*
Department of Chemical and Biomolecular Engineering, Rice University, Houston, TX, USA

*Corresponding author: E-mail: biswal@rice.edu

Supplementary Video 1: Dislocation glide, reflection, and nucleation from extensional and compressive stresses within monodisperse wet foam (1 mL h^{-1} and 500 mbar, $\Phi = 0.94$, bubble diameter ≈ 125 μm) subjected to expansion-contraction flow at 200 fps (recorded at 400 fps). In order of first materialization: dislocation-union reflection in tension (Fig. 8a-e), $\vec{b}_2$ nucleation (Fig.12), reflection in compression (Fig. 11), dislocation-split reflection (Fig. 8i-iv) transitioning to multi-stage reflection (similar to Fig. S1), and dislocation reflection in the bulk (Fig. 10). The misaligned state of Fig. 4a is at 24 seconds of playback.

Supplementary Video 2: Dislocation glide, reflection, and nucleation from extensional and compressive stresses within monodisperse wet foam (1 mL h^{-1} and 500 mbar, $\Phi = 0.94$, bubble diameter ≈ 125 μm) subjected to expansion-contraction flow at 200 fps (recorded at 400 fps). In order of first materialization: dislocation gliding in the compression rearrangement zone combining by vector addition with dislocation gliding near the wall that resulted from reflection in the bulk downstream (outside of the field of view), hopping (Fig. 9), reflection in compression (Fig. 11) at the sinusoidal wall, standard reflection in tension (Fig. 7) at the sinusoidal wall, and dislocation glide from $\vec{b}_2$ nucleation upstream (outside of the field of view). The aligned state of Fig. 4b is at 13 seconds of playback.

Fig. S1: A still image of foam in the model crystalline system (1 mL h^{-1}, 500 mbar and $\Phi = 0.94$) with a bounding box from peak to peak of the sinusoidal wall (4000 μm) representing the control volume used to calculate the scaled T1 event count: $P_{T1} = N_{T1}/N_{bubbles}$. Scale bar is 250 μm (roughly two bubble diameters).

Fig. S2: A multi-stage reflection in tension at the sinusoidal wall (1 mL h^{-1}, 500 mbar and $\Phi = 0.94$). The total elapsed time is 60 ms. Scale is roughly 250 μm per two bubble diameters.

Fig. S3: A $-\vec{b}_1$ breakup reaction in the bulk of the foam due to compressive forces in the contraction region (1 mL h^{-1}, 500 mbar and $\Phi = 0.94$). The total elapsed time is 45 ms. Scale is roughly 250 μm per two bubble diameters.

Fig. S4: Formation of a 5/5 $\vec{b}_1$ dislocation dipole from two dislocations with $\vec{b}_2$ orientation and subsequent dissociation *via* an intermediate ring structure consisting of three dislocation pairs around a triangular-shaped central bubble (1 mL h^{-1}, 500 mbar and $\Phi = 0.94$). The total elapsed time is 70 ms. Scale is roughly 250 μm per two bubble diameters.

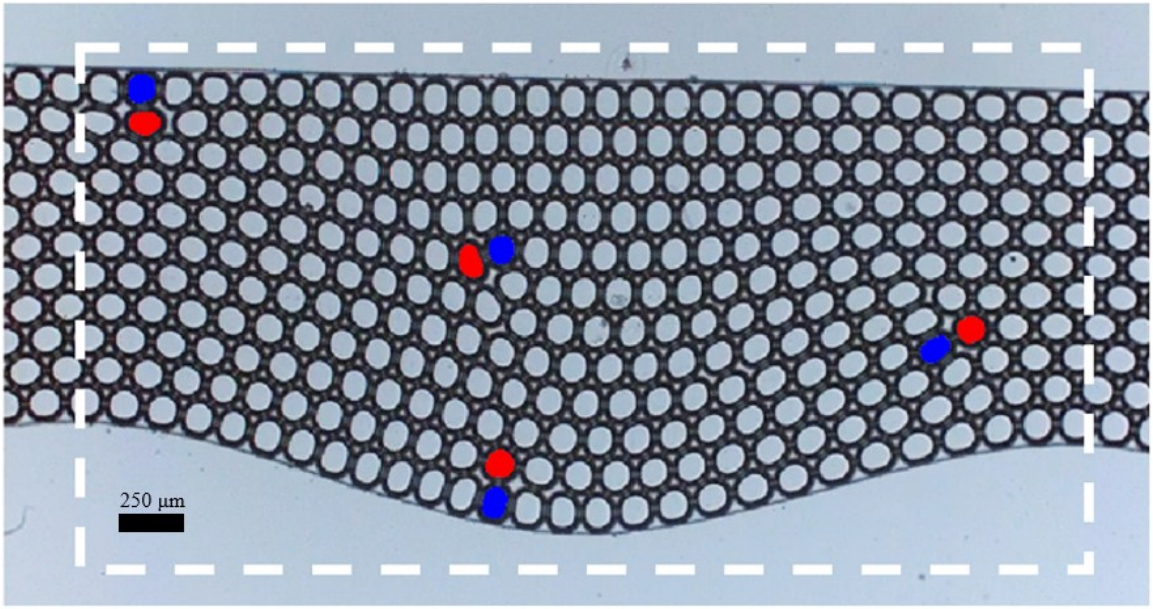

Fig. S1: A scaled T1 event count was defined as $P_{T1} = N_{T1}/N_{bubbles}$ (the number of T1 events per bubble) in a similar fashion as previously performed for drops in a tapered microfluidic channel.[1] However, a major difference in the present calculation compared with the previous emulsion work was that the control volume for observing the number of T1 events and bubbles was the length of the channel from peak to peak (see dashed white box above) rather than an individual rearrangement zone. In the model crystalline system (1 mL h^{-1} surfactant solution, 500 mbar air), 300 ± 5 bubbles were contained within the control volume (as measured by the bubble centroids) for each frame. The time required for 300 bubbles to advect past the downstream edge of the control volume was measured and the corresponding number of T1 events within the control volume in that timeframe (roughly 0.26s) was recorded. P_{T1} was calculated with $N_{bubbles} \approx 600$ (i.e. double the peak to peak bubbles as the control volume is effectively replaced with a new set of bubbles in that time interval). $P_{T1} = 0.33 \pm 0.03$ for the model crystalline system was determined after tracking a total of 3000 bubbles. The corresponding value in the tapered microfluidic channel for the same value of the capillary number ($Ca \sim 10^{-4}$) was roughly 0.2.[1] The difference in P_{T1} can be attributed to the altered definition of the control volume, the dissimilar geometry of the microfluidic channel, and the extended dislocation mechanisms exhibited in the present work compared with the previous emulsion study[1] (e.g. reflection in tension is conservative, generating an additional dislocation compared with the exclusively observed reflection in compression in the tapered channel).

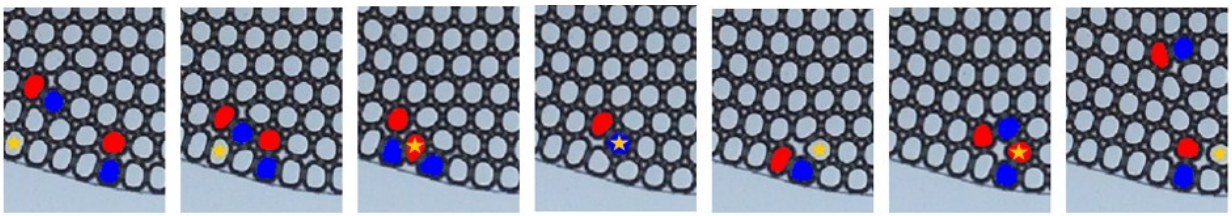

Fig. S2: (a-c) A hopping event[2] occurs after bubbles of the $-\vec{b}_2$ and $\vec{b}_1$ dislocation become neighbors. The (starred) wall bubble between the 5/7 neighbor pair of the $-\vec{b}_2$ dislocation hops into the adjacent row due to the high energy free space resulting from the dislocation positioned at the wall and the retreating seven-neighbor (red) bubble of the $-\vec{b}_2$ dislocation. Under these conditions, hopping does not displace an additional bubble from the adjacent row into the third row as in instances at the horizontal wall (see Fig. 9). (d) Hopping eliminates the dislocation at the wall and forms a new $-\vec{b}_2$ dislocation shifted one bubble in the positive first direction (against the direction of foam flow). (e-g) The new dislocation undergoes standard reflection, $-\vec{b}_2 \rightarrow \vec{b}_1 + \vec{b}_3$. The extended wall bubble (colored red in part e) is forced against the wall and the $3_w/7$ dislocation shifts back along the positive first direction.

(not shown) A second hopping can occur and prevent the standard reflection. In the case of two consecutive hops, the second hop proceeds in a similar manner to hopping at the horizontal wall with the additional bubble displacement (see Fig. 9). The dislocation destroyed by the first hopping event is not replaced due to the nonconservative reflection. The reflected dislocation is shifted by two bubbles in the positive first direction compared to a standard reflection without hopping.

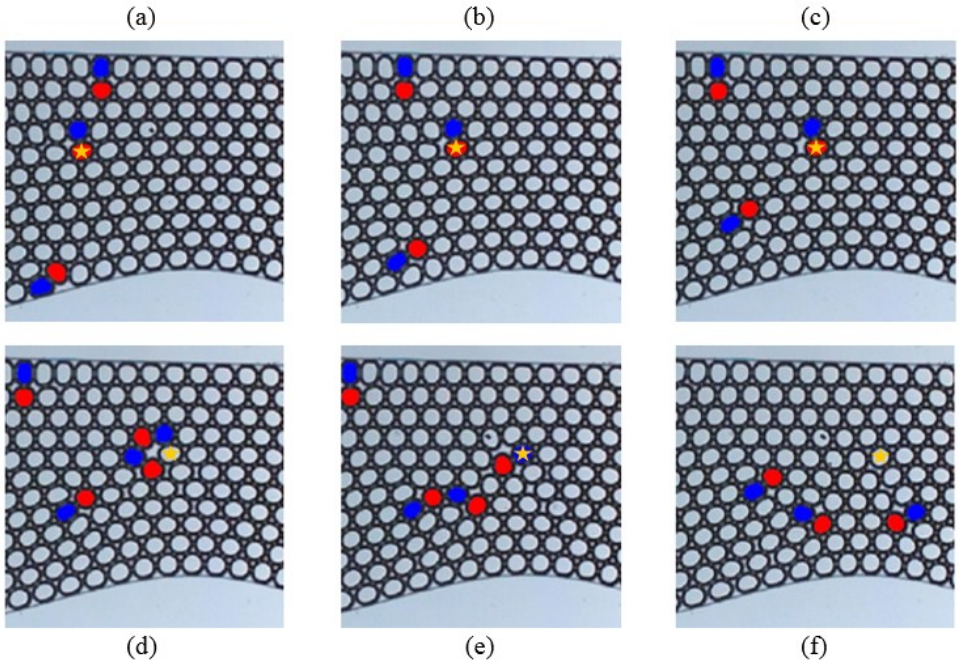

Fig. S3: (a-b) A $-\vec{b}_1$ dislocation created from dislocation reflection in the bulk approaches the contraction from a combination of dislocation glide (not shown) and advection of the bubbles comprising the dislocation. (b-c) The compressive forces in the region of the contraction squeeze the bubbles of the dislocation and the interstitial space upstream increases in size. Strain rates for these bubbles prior to the T1 topological rearrangement responsible for breakup were calculated around 20 s^{-1} in the model system using PIVlab.[3] (c-d) A T1 topological rearrangement occurs as the seven neighbor bubbles in part (d) converge along the direction of compression. (e-f) The conservative breakup reaction can be expressed as $-\vec{b}_1 \rightarrow \vec{b}_2 + \vec{b}_3$. The $\vec{b}_3$ dislocation glides opposite the direction of the Burgers vector into the region of reduced packing density near the sinusoidal wall. Strain rates from these breakup events were calculated[2] as high as 50 s^{-1} in the model system.

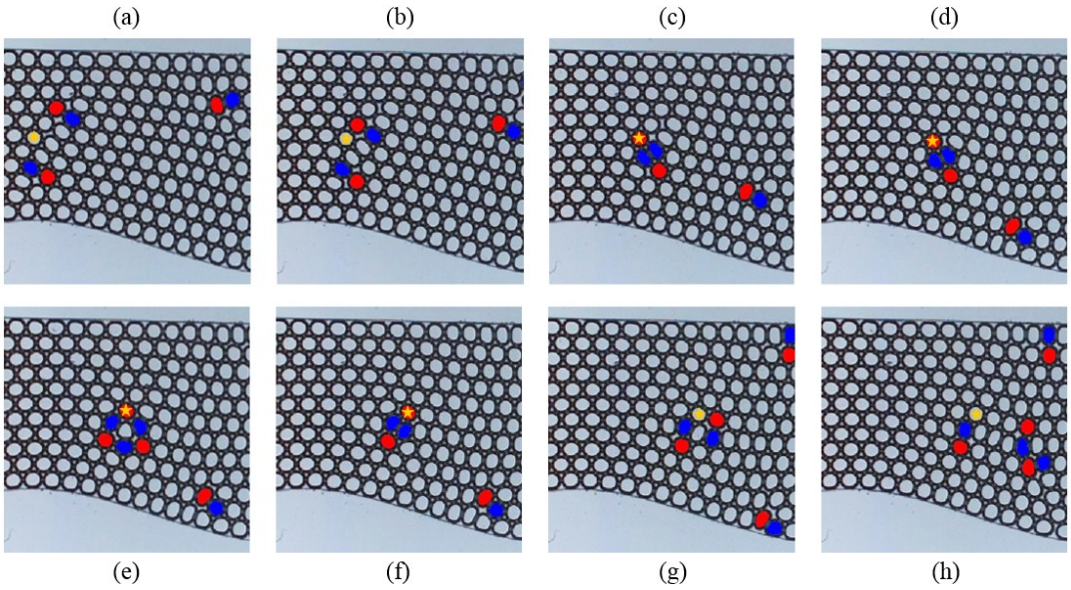

Fig. S4: As dipoles have reduced local packing densities, additional complexities in the temporal progression often occur for conditions at or below the gas area fraction of the model system (shown above). (a-b) Two dislocations with $\vec{b}_2$ orientation glide towards each other. The slanted orientation of the bubble rows in the region downstream of the contraction misalign the bubbles between and comprising the two dislocations (note the characteristic orientation of the perfectly packed crystal in the same region of the channel for the other subfigures). The bubbles are more vertically orientated in comparison to conditions with higher Φ (see Fig. 15a,b for the orientation of the foam prior to and upon formation of a 5/5 $\vec{b}_2$ dislocation dipole at a comparable location). (c-d) The 5/5 dipole (resembling the ISW defect in graphene[4,5]) forms with $\vec{b}_1$ (rather than $\vec{b}_2$) orientation as the dislocations swap five-neighbored bubbles. (e) A T1 topological rearrangement occurs as the upstream semicircular bubbles proximal to the dipole diverge along the direction of tension in the positive third direction (see Fig. 15e,f where the analogous T1 topological rearrangement results in direct dissociation of the dipole when one of the diverging bubbles is part of the dipole). An intermediate six-membered ring structure forms (resembling the partially dissociated ISW defect in graphene[5,6]). (e-f) A second T1 topological rearrangement occurs as the central bubble inside the ring diverges with the bubble in the positive third direction and a new 5/5 $\vec{b}_1$ dislocation dipole forms. The dislocations have passed through each other (the starred dislocation formerly on the upstream side of the dipole now resides on the downstream side). (g-h) These $\vec{b}_1$ dislocations separate and move away from one another against the respective gliding directions due to local flow conditions and interactions with nearby dislocations. The sequence of events following the formation of a 5/5 $\vec{b}_1$ dislocation dipole is analogous when the dipole forms from two $\vec{b}_1$ dislocations in the same region of the channel.

(not shown) $\vec{b}_1$ dislocations can glide towards each other following separation and reform a dipole. More complex progressions as a result of reduced packing density, nearby dislocations along a slip plane, and/or transitioning alignment (curvature) of the bubble rows from expansion-contraction flow can result in formation of a dipole having different orientation than the initial dipole after (or without) an intermediate ring configuration. As in cases of dislocation pass through, the reformed dipole is always comprised of two of the same bubbles of the initial dipole.

References

1. Y. Gai, A. Bick and S. K. Y. Tang, *Phys. Rev. Fluids*, 2019, **4**, 014201.
2. M. E. Rosa and M. A. Fortes," *Philos. Mag. A*, 1998, **77**, 1423–1446.
3. W. Thielicke and E. J. Stamhuis, *J. Open Res. Software*, 2014, **2**, e30.
4. M. T. Lusk and L. D. Carr, *Phys. Rev. Lett*., 2008, **100**, 175503.
5. M. T. Lusk, D. T. Wu and L. D. Carr, *Phys. Rev. B*, 2010, **81**, 155444.
6. M. T. Lusk and L. D. Carr, *Carbon*, 2009, **47**, 2226–2232.